IEEE Open Journal of
Power Electronics

Received 29 August 2023; revised 14 October 2023; accepted 22 October 2023. Date of publication 27 October 2023;
date of current version 22 November 2023. The review of this article was arranged by Associate Editor Chandan Kumar.

Digital Object Identifier 10.1109/OJPEL.2023.3328112

Detailed Parametric Modeling of AC–DC Converters for EMT Simulators

PARASTOO SADAT HOSSEINIAN (Student Member, IEEE), SEYYEDMILAD EBRAHIMI (Member, IEEE), AND JURI JATSKEVICH (Fellow, IEEE)

Department of Electrical and Computer Engineering, The University of British Columbia, Vancouver, BC V6T 1Z4, Canada

CORRESPONDING AUTHOR: SEYYEDMILAD EBRAHIMI (e-mail: ebrahimi@ece.ubc.ca)

This work was supported by the Natural Science and Engineering Research Council (NSERC) of Canada under the Collaborative Research and Development Grant.

ABSTRACT Detailed switching models of ac–dc converters are available in many offline and real-time electromagnetic transient (EMT) simulation programs. However, such discrete models typically require small simulation time steps for accurately handling the switching events without interpolation. This paper proposes a new parametric modeling approach for line-commutated and 2-level voltage-source ac–dc converters. The proposed methodology is based on parametric functions that relate ac and dc variables in the instantaneous sense, which allows the reconstruction of the waveforms of voltages and currents (with the same level of details as the switching models of converters) without topological changes in the converter circuit. Thus, it can operate at larger time steps without requiring interpolation, thereby enhancing simulation efficiency. The computational advantages of the proposed models over the conventional switching models are demonstrated in offline PSCAD and real-time RTDS NovaCor simulators in terms of maximum possible time step size and accuracy. It is shown that the proposed models can accurately run with much larger time steps (up to $\sim$200 μs for LCRs, and up to $\sim$50 μs for VSCs) compared to detailed switching models, which are limited to relatively small time steps of $\sim$10 μs.

INDEX TERMS Ac–dc converter, interfacing, line-commutated, modeling, nodal analysis, real-time, simulation, switching, VSC.

I. INTRODUCTION

Power-Electronic converters play an important role in modern energy systems by connecting new energy resources to conventional power grids. In many applications, the 2-level diode/thyristor-based line-commutated rectifiers (LCRs) and voltage-source converters (VSCs) are used as basic building blocks due to the simplicity and reliability of this technology [1], [2]. Such applications include the classic HVDC transmission systems [3], [4], [5], power systems of vehicles [6], [7], ships and aircraft, induction furnaces [8], excitators of synchronous generators [9], [10], [11], etc.

The LCRs and VSCs also produce ac harmonics and dc ripples [12], [13], which may affect other components in the power system [14]. Therefore, offline and real-time electromagnetic transient (EMT) simulations of systems with such converters are often conducted to analyze waveforms of ac and dc terminal variables, design harmonic filters, etc.

For such purposes, the conventional detailed switching models of these ac-dc converters are typically available as standard library components in many commercial EMT simulation programs. Such switching models offer accurate solutions by considering the operation of every semiconductor device individually. However, these models typically require significant computing resources due to many discrete switching events that need to be detected and processed [15]. For example, offline programs may apply interpolation and zero-crossing detection to facilitate simulations with larger time steps without compromising accuracy. This can help eliminate (numerical) voltage spikes and/or chatter in systems with VSC circuits, etc., avoiding the need for unrealistic snubber circuits for numerical damping [16]. Additionally, they can allow precise modeling of non-characteristic harmonics originating from switching devices [17], etc.

However, interpolations can be numerically costly and impractical for real-time simulation [18]. Consequently, while

some switching prediction algorithms [19], [20] have been developed for real-time EMT programs, they often need small time-step sizes for simulations to handle the switching events. This makes detailed switching models (DSMs) of converters simulation bottlenecks for system-level studies with many switching components. For example, this may result in a very long run time in offline simulations; or cause time-step overflow (i.e., overrun) in real-time simulations when the computations in each step exceed the time-step window [21], [22].

To avoid the computational cost of DSMs, efficient alternatives, such as the dynamic phasor models [23]–[26] and average value models (AVMs) [27], [28], [29], [30], [31], [32], [33], have been developed. These models facilitate the simulation of large-scale power systems by adopting larger time steps at the cost of neglecting the switching details of individual semiconductor devices. The parametric AVMs (PAVMs) [34], [35], [36] were developed for LCRs, and have proven accurate under various operating conditions. In PAVMs, algebraic formulations are used to relate the average values of the dc-side and ac-side transformed variables (in *qd* coordinates) using the so-called parametric functions that are obtained numerically [34]. A generalized PAVM (GPAVM) for LCRs was presented in [37] that is able to reconstruct selected harmonics of the ac variables in addition to their fundamental frequency components (by transforming them into multiple *qd* reference frames corresponding to different selected harmonics). Including more harmonics increases the complexity of the GPAVM. To reduce this complexity, a hybrid PAVM/detailed model (HPAVM) of LCRs was proposed in [38], which uses only one *qd* transformation. This was done using extra parametric functions for the oscillatory components for reconstructing ac harmonics and dc ripples as accurately as the DSMs. However, in the HPAVM, the harmonics of the ac variables and the ripples of the dc variables are computed separately from their fundamental frequency components and averages, respectively, which comes with an additional computational cost.

The AVMs, PAVMs, GPAVM, and HPAVM are typically interfaced with the external networks using controlled voltage/current sources [33], [34], [35], [36], [37], [38]. Some state-variable-based programs [39] can solve the external network simultaneously with the AVMs. However, in EMTP-type programs with non-iterative solution (e.g., PSCAD), one time-step delay between the solution of the external network and the AVM interfacing variables is applied inevitably by the program [40] (referred to as indirect interfacing). This delay may cause numerical inaccuracy or instability at large simulation time steps.

Direct interfacing techniques have been developed in [41] and [42] for AVMs of LCRs and VSCs in the nodal analysis-based solution, eliminating the interfacing time-step delay. This was done by linearizing the average-value relations and formulating a conductance matrix for the LCR PAVM and VSC AVM to be solved as part of the overall network solution. However, the directly interfaced methods are based on the classic AVM of the converters and are only able to preserve the fundamental frequency components of the ac waveforms and the average values of the dc variables.

This paper proposes a new parametric detailed non-switching model (DNSM) for the widely-used 2-level ac-dc converters, i.e., LCRs and VSCs. The contributions of this paper and the features of the new modeling technique are summarized as follows:

- The proposed DNSM is able to reconstruct the ac and dc waveforms similar to the DSMs of converters, including all harmonics and ripples. This is achieved by formulating the parametric functions defined based on the instantaneous values of ac and dc variables. This is a fundamental departure from all previous parametric AVMs [33], [34], [35], [36], [37], [38], including the GPAVM and HPAVM, which are based on average-value relationships.
- Two interfacing methodologies for DNSM, denoted as indirectly-interfaced DNSM (IDI-DNSM), which uses a time-step relaxation, and directly-interfaced DNSM (DI-DNSM), which uses linearization and simultaneous solution [41], are formulated.
- The advantages of the proposed models over the DSMs are demonstrated on generic LCRs and VSCs implemented in PSCAD (offline simulations) and RSCAD (real-time simulations using NovaCor of RTDS). It is verified that IDI-DNSM and DI-DNSM allow much larger simulation time steps compared to the conventional DSMs while providing accurate waveforms for ac and dc variables.

II. DETAILED PARAMETRIC MODEL OF AC-DC CONVERTERS

Without loss of generality, a generic three-phase 2-level ac–dc conversion system depicted in Fig. 1 is considered to define the proposed methodology. The ac and dc subsystems are interconnected by either a six-pulse LCR (composed of diode or thyristor switches) or a VSC (composed of forced-commutated transistors, e.g., IGBTs). The dc subsystem may consist of a dc network and an optional low-pass filter to smoothen the dc terminal voltage. The ac subsystem may include rotating electrical machines, ac filters, ac loads, transmission lines, etc. The Thévenin equivalent is utilized to represent the ac subsystem where equivalent voltages $\mathbf{e}_{abc}$ are assumed to be balanced and sinusoidal as

$$\mathbf{e}_{abc} = \sqrt{2}\,E_{\text{rms}}\left[\cos(\theta_s) \quad \cos\left(\theta_s - \tfrac{2\pi}{3}\right) \quad \cos\left(\theta_s + \tfrac{2\pi}{3}\right)\right]^T. \tag{1}$$

Here, E_{rms} is the rms value of phase voltages, and θ_s indicates the angle of phase a of the equivalent ac sources. The ac side Thévenin equivalent impedance is represented by r_s and L_s. The converter terminal voltages are denoted by $\mathbf{v}_{abc}$ whose fundamental frequency component has the angle

$$\theta_e = \int (2\pi f_e)\, dt, \tag{2}$$

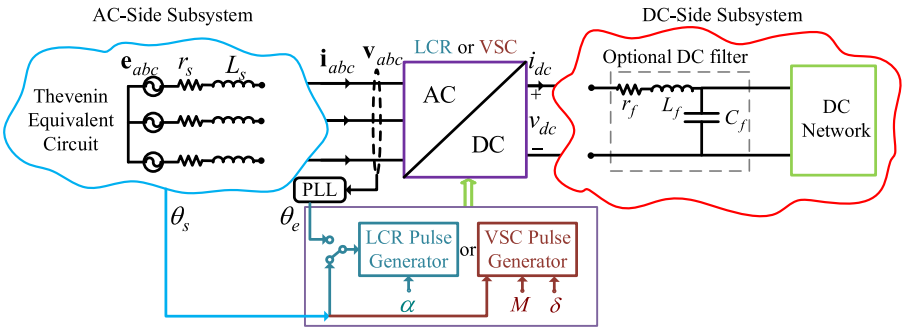

FIGURE 1. Generic ac–dc converter system consisting of an LCR or VSC.

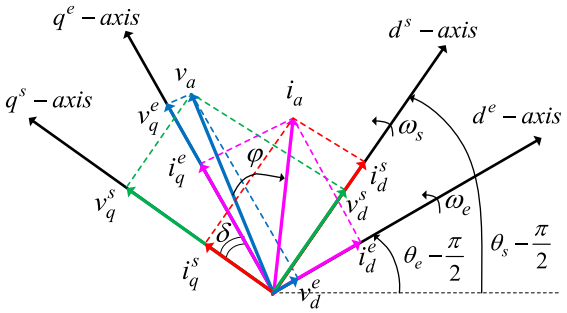

FIGURE 2. Vector diagram of the converter ac currents and voltages in two *qd* reference frames rotating with angles of ac sources and converter terminal voltages.

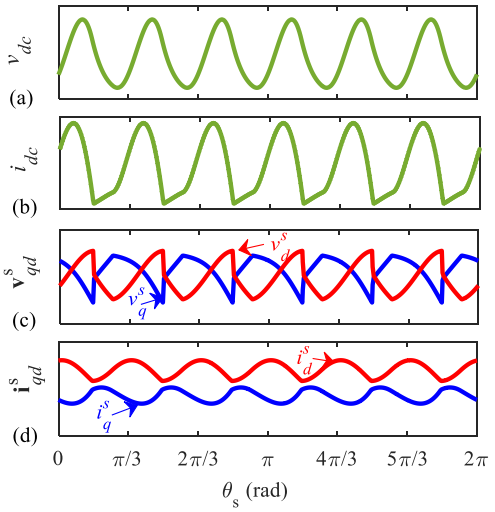

FIGURE 3. Typical waveforms of terminal variables for six-pulse LCRs over one ac cycle: (a) dc voltage, (b) dc current, (c) ac transformed *qd* voltages, (d) ac transformed *qd* currents.

where f_e is the frequency of the ac subsystem in Hz. The angles θ_e and θ_s are related as

$$\delta = \theta_s - \theta_e, \tag{3}$$

where δ is referred to as the power transfer angle.

As depicted in Fig. 1, the firing angle α and angle θ_s, or θ_e, are the inputs into the firing pulse generator for the thyristor-based LCRs. The firing angle α may be computed with respect to either the angle θ_s or θ_e, which can be identified by a phase-locked-loop (PLL). For the VSC, the modulation index M, angle δ, and angle θ_s are the inputs into the pulse generator. Here, δ is used to specify the angle of the fundamental frequency component of the VSC ac voltages θ_e based on (3). Also, the modulation index M determines the amplitude of the fundamental frequency component of VSC ac voltages with respect to the dc terminal voltage.

A. FORMULATION OF DNSM

For the purpose of derivation, the converter ac voltages $\mathbf{v}_{abc}$ and currents $\mathbf{i}_{abc}$ are transformed to the source *qd* synchronous reference frame with angle θ_s, as shown in Fig. 2, and computed using Park's transformation matrix $\mathbf{K}$ [4] as

$$\mathbf{v}^s_{qd} = \mathbf{K}(\theta_s)\mathbf{v}_{abc}, \qquad \mathbf{i}^s_{qd} = \mathbf{K}(\theta_s)\mathbf{i}_{abc}, \tag{4}$$

where $\mathbf{v}^s_{qd}$ and $\mathbf{i}^s_{qd}$ are the transformed ac variables. In the source *qd* reference frame, the axis q^s is aligned with the phase *a* of the equivalent source voltages $\mathbf{e}_{abc}$.

Typical waveforms of dc and transformed *qd* ac variables for the LCR-based ac-dc system in Fig. 1 are illustrated in Fig. 3. As seen in Fig. 3, similar to the dc-side variables, the transformed *qd* ac variables are also composed of dc average values and oscillatory components (i.e., ripples) which correspond to the sum of all the ac harmonics in the *abc* coordinates. Also, the dc average values of *qd* variables correspond to the amplitude of the fundamental frequency component of the ac variables in the *abc* coordinates.

In the VSC-based system, the dc and *qd* variables also contain dc average values and ripples generated by the high-frequency switching. Their average values will correspond to the fundamental frequency components, and the ripples will correspond to the ac harmonics.

The proposed technique captures the relationships between the entire waveforms of the dc and *qd* ac variables using parametric functions structured similarly to the conventional parametric functions [34], [38]. However, as opposed to all previous PAVM [34], GPAVM [37], and HPAVM [38], in the proposed DNSM, these relationships are formulated based on the instantaneous values of the dc and *qd* ac variables/waveforms. For this purpose, a parametric function

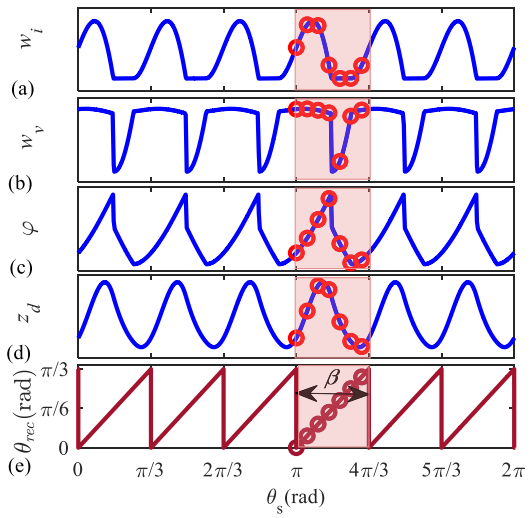

FIGURE 4. Typical waveforms of the instantaneous parametric functions and dynamic impedance of the LCR-based system for the proposed DNSM over one ac cycle: (a) parametric function w_i(.) defined in (5), (b) parametric function w_v(.) defined in (6), (c) parametric function φ(.) defined in (7), (d) dynamic impedance z_d defined in (8), and (e) reconstruction angle θ_{rec} defined in (11).

$w_i(.)$ is defined as

$$w_i(.) = \frac{i_{dc}}{\left\| \mathbf{i}^s_{qd} \right\|}, \tag{5}$$

which at any moment relates the instantaneous values of the dc current and the magnitude of the qd ac currents. Similarly, a parametric function $w_v(.)$ is defined as

$$w_v(.) = \frac{\left\| \mathbf{v}^s_{qd} \right\|}{v_{dc}}, \tag{6}$$

which at any moment relates the instantaneous values of the dc voltage and the magnitude of the qd ac voltages.

The phase shift between the instantaneous angles of the ac currents and ac voltages is also captured with a parametric function $\varphi(.)$ defined as

$$\varphi(.) = \tan^{-1}\left(\frac{i^s_d}{i^s_q}\right) - \tan^{-1}\left(\frac{v^s_d}{v^s_q}\right). \tag{7}$$

The parametric functions (5)–(7) are defined at any moment and for the desired operating conditions of the ac-dc converter. For this purpose, the loading condition of the converter is specified by defining an instantaneous dynamic impedance as

$$z_d = \frac{v_{dc}}{\left\| \mathbf{i}^s_{qd} \right\|}. \tag{8}$$

The profiles of the parametric functions $w_i(.)$, $w_v(.)$, $\varphi(.)$, and z_d calculated based on the typical waveforms in Fig. 3 for the LCR system are depicted in Fig. 4 over one ac cycle. It is observed that these functions are also periodic, similar to the ripples on the dc and qd ac variables when considering their instantaneous values. The period of these ripples for an LCR-based system is obtained as [38]

$$\beta = 2\pi/p, \tag{9}$$

where p denotes the number of LCR pulses (in Figs. 3 and 4 $p = 6$).

For VSCs, the period of ripples β on the dc and qd variables, and parametric functions is equal. However, β of VSCs will also depend on the switching strategy, unsynchronized or synchronized carrier frequency, symmetry or asymmetry of the carrier about a sinusoidal reference waveform of SPWM, etc. [1], [44].

In this article, a synchronous modulation with odd and multiple of 3 switching frequency ratio is considered to eliminate the even and triple harmonics, and the harmonics of the order of the carrier frequency, resulting in the ac harmonic order of [45]

$$n = 6m \pm 1, \quad m \in \{1, 2, 3, \ldots\}, \tag{10}$$

which results in the harmonic order of $6m$ on dc and qd variables. Therefore, the period of ripples is specified as $\beta = \frac{\pi}{3}$ for the subject VSC system [45].

After determining the period β, adequate samples of the parametric functions can be collected over only one period β as illustrated in Fig. 4. For this purpose, the so-called reconstruction angle θ_{rec} is defined as [38]

$$\theta_{rec} = \text{mod}\ (\theta_s/\beta). \tag{11}$$

The profile of θ_{rec} is shown in Fig. 4(e).

B. ESTABLISHING PARAMETRIC FUNCTIONS

It is generally impractical to derive the instantaneous parametric functions (5)–(7) analytically under various operating conditions, especially when considering the nonlinearity and losses of the converter. Here, Algorithm 1 is used to numerically establish the parametric functions of the LCR-based ac–dc system. A similar approach is used for constructing parametric functions of the VSC-based system.

In this approach, the system is simulated using the DSM of the converter for short periods of time over different loading conditions, and the parametric functions are computed numerically. As shown in Algorithm 1, the system is simulated over the desired range of firing angles (in the case of thyristor-based LCR) denoted by its minimum $\alpha_{\min}$ and maximum $\alpha_{\max}$ values with step α_{step}.

The system is also simulated over the desired range of loading conditions. Here, the loading condition is varied by changing the load in the dc network, which is represented by an equivalent resistance R_l, which steps with $R_{l,\text{step}}$ from minimum $R_{l,\min}$ to maximum $R_{l,\max}$. It is important to note that the parametric functions obtained by varying a resistive load in the dc network are also valid for other load compositions in the dc networks, such as inductive loads.

Once the simulations start, the parametric functions are computed based on (5)–(7). Also, the dynamic impedance z_d and the reconstruction angle θ_{rec} are also established based on (8), (11), respectively, for that operating condition. Then,

Algorithm 1: Algorithm for Construction of Lookup Tables.

1. **for** $\alpha = \alpha_{\min}$ **to** $\alpha_{\max}$ **step** α_{step} **do**
2. **for** $R_l = R_{l,\min}$ **to** $R_{l,\max}$ **step** $R_{l,\text{step}}$ **do**
3. Initialize the system with α and R_l using DSM for LCR
4. Start the simulation
5. **for** $k = 0$ **to** N **step** 1 **do**
6. Establish θ_{rec} based on (11)
7. Compute functions $w_i(.)$, $w_v(.)$, $\varphi(.)$ based on (5)–(7)
8. Compute dynamic impedance z_d based on (8)
9. Store the parametric functions in 3-D lookup tables in terms of z_d, α, θ_{rec}
10. **end for**
11. End the simulation
12. **end for**
13. **end for**

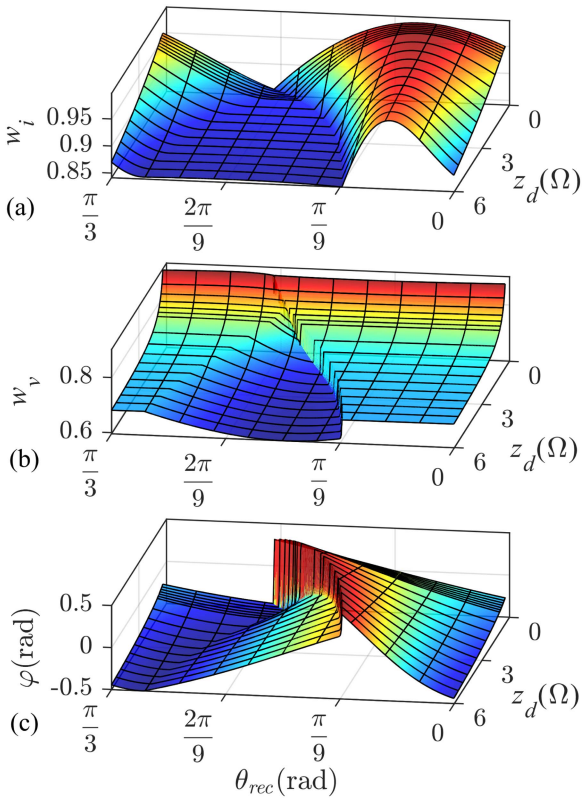

FIGURE 5. Typical parametric functions for the proposed DNSM of a diode rectifier stored in lookup tables: (a) $w_i(.)$, (b) $w_v(.)$, and (c) $\varphi(.)$.

N samples of the parametric functions are collected over one period β, and stored in three-dimensional (3-D) lookup tables in terms of α (for thyristor-based LCR), z_d, and θ_{rec}. Typical profiles of instantaneous parametric functions for the proposed DNSM of a diode rectifier are shown in Fig. 5.

For the VSC system, applying the same Algorithm 1, four-dimensional (4-D) lookup tables in terms of modulation index M, angle δ, z_d, and θ_{rec} are constructed and stored as the instantaneous parametric functions over the desired range of operation.

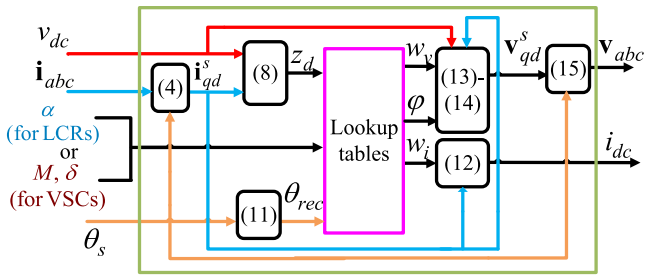

FIGURE 6. Implementation of the proposed DNSM using indirect interfacing with external networks.

It is noted that the construction time and size of the lookup table data are determined by the desired resolution of parametric functions and the range of operating conditions. This is a one-time procedure, and once the lookup tables are established, they can be used for various studies.

It should be noted that linear interpolation is used to predict the output value when an input of the lookup tables (e.g., firing angle for thyristor-based LCRs or modulation index and angle for VSCs) falls between two stored values. This enables a more precise extraction of the values of parametric functions for various conditions during simulations, providing the ability to respond to the outputs of control systems effectively.

III. INTERFACING METHODS

Once the parametric functions are established as lookup tables, the proposed DNSM is readily implemented, as shown in Fig. 6. As seen, the firing angle α (in case of thyristor-based LCR) or modulation index M and angle δ (in case of VSC), the source angle θ_s, the dc voltage v_{dc}, and the ac currents $\mathbf{i}_{abc}$ are the inputs to the DNSM. The ac voltages $\mathbf{v}_{abc}$ and the dc current i_{dc} are the outputs.

According to Fig. 6, the currents $\mathbf{i}_{abc}$ coming from the external system are transformed to the qd coordinates based on (4). Then, z_d and θ_{rec} are computed based on (8), (11) using the input variables v_{dc}, θ_s, and $\mathbf{i}^s_{qd}$. The values of z_d and θ_{rec} are then used along with the LCR firing angle α (or VSC modulation index M and angle δ) as the inputs to the lookup tables to compute the values of parametric functions $w_i(.)$, $w_v(.)$, and $\varphi(.)$. Afterward, the value of the output dc current is calculated based on (5) using $\mathbf{i}^s_{qd}$ and $w_i(.)$ as

$$i_{dc} = w_i(.) \left\| \mathbf{i}^s_{qd} \right\|. \tag{12}$$

Also, the converter output ac voltages in qd coordinates are calculated based on (6), (7) using the inputs v_{dc}, $\mathbf{i}^s_{qd}$, and the computed parametric functions $w_v(.)$ and $\varphi(.)$ as

$$v^s_q = w_v(.)\, v_{dc} \cos\left(\tan^{-1}\left(\frac{i^s_d}{i^s_q}\right) - \varphi(.)\right), \tag{13}$$

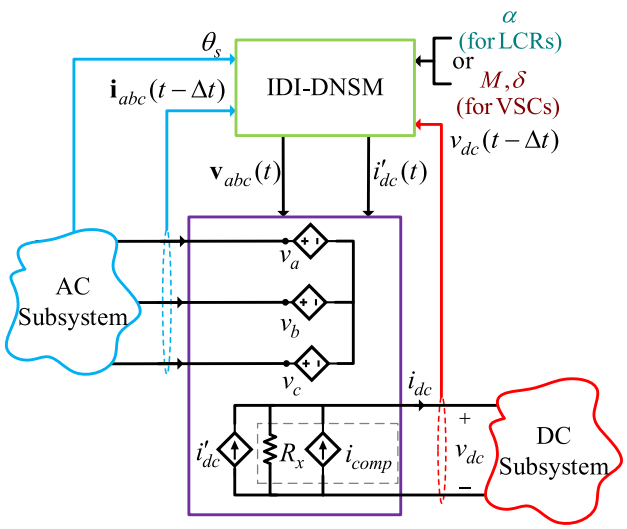

FIGURE 7. Indirect interface of the proposed DNSM with the external network using controlled current and voltage sources.

$$v_d^s = w_v(.)\, v_{dc} \sin\left(\tan^{-1}\left(\frac{i_d^s}{i_q^s}\right) - \varphi(.)\right). \tag{14}$$

Finally, the *abc* voltages are computed using the inverse of Park's transformation matrix as

$$\mathbf{v}_{abc} = [\mathbf{K}(\theta_s)]^{-1}\mathbf{v}_{qd}^s. \tag{15}$$

A. INDIRECT INTERFACING METHOD USING CONTROLLED SOURCES

To interface the proposed DNSM with external networks using circuit components, the discrete switches of the converter are replaced with dependent voltage and current sources, as depicted in Fig. 7. Therein, the three-phase voltage sources are used to interface the output $\mathbf{v}_{abc}$ with the ac subsystem, and the controlled intermediate dc current source, calculated based on (12), is used to interface the output i'_{dc} with the dc subsystem.

As shown in Fig. 7, depending on the composition of the dc subsystem, a snubber resistor R_x may be needed in parallel with the dc current source i'_{dc} when the dc subsystem cannot accept the current source at the inputs (e.g., when there is a line inductor in series with the dc current source) [46]. If a snubber is used, a compensation current source i_{comp} should be used to eliminate the steady-state error caused by the snubber current. To achieve an explicit and non-iterative interface, the compensation current i_{comp} is calculated using the input dc voltage from the previous time-step as

$$i_{comp}(t) = \frac{v_{dc}(t-\Delta t)}{R_x}. \tag{16}$$

In EMTP-type programs without an iterative solution, e.g., PSCAD and RSCAD, the inputs to the DNSM block (i.e., dc terminal voltage v_{dc} and the ac currents $\mathbf{i}_{abc}$ in Figs. 6 and 7) use their values from the previous time-step (i.e., $v_{dc}(t-\Delta t)$ and $\mathbf{i}_{abc}(t-\Delta t)$) since their values are not computed at the present time-step yet.

The method presented here is referred to as indirect interfacing due to using the time step delay in the interfacing variables. The interfacing delay can cause numerical inaccuracy and instability in simulations with large time steps. Therefore, the proposed indirectly-interfaced DNSM (IDI-DNSM) may not be able to run with large time-step sizes, although it still allows larger time-step sizes compared to the DSMs of converters.

B. DIRECT INTERFACING FOR THE PROPOSED DNSM

Inspired by [41], a direct interfacing method is developed for the proposed DNSM. The proposed directly-interfaced DNSM (DI-DNSM) is aimed to allow large time-step sizes in EMTP-type programs without the need for iterative interfacing solutions. To eliminate the one-time-step delay, the DNSM of the ac-dc converter is reformulated in the nodal solution form so that its resultant matrices and vectors can be merged with the overall network solution and solved simultaneously without a time-step delay.

The nodal equation of the overall system, including the converter, has the following general form

$$\begin{matrix} \mathbf{G} & \mathbf{V} & \mathbf{I} \end{matrix}$$
$$\begin{bmatrix} \vdots & \\ \cdots & \mathbf{G}_{\mathrm{CON}} \\ \vdots & \end{bmatrix} \begin{bmatrix} \vdots \\ \mathbf{V}_{\mathrm{CON}} \\ \vdots \end{bmatrix} = \begin{bmatrix} \vdots \\ \mathbf{I}_{h\mathrm{CON}} \\ \vdots \end{bmatrix}, \tag{17}$$

where $\mathbf{V}$ is the vector of system nodal voltages, $\mathbf{G}$ is the system's conductance matrix, and the vector $\mathbf{I}$ represents the sum of injected currents to the nodes, including history currents and independent sources. Similarly, $\mathbf{G}_{\mathrm{CON}}$ is the conductance sub-matrix of the converter DNSM model, whose voltages are defined in a vector form as

$$\mathbf{V}_{\mathrm{CON}} = [v_a(t) \quad v_b(t) \quad v_c(t) \quad v_{dc}(t)]^T. \tag{18}$$

The converter currents are defined in vector form as

$$\mathbf{I}_{\mathrm{CON}} = [i_a(t) \quad i_b(t) \quad i_c(t) \quad i_{dc}(t)]^T. \tag{19}$$

The vector of history currents is defined as

$$\mathbf{I}_{h\mathrm{CON}} = \left[i_{ha}(t) \quad i_{hb}(t) \quad i_{hc}(t) \quad i_{hdc}(t)\right]^T. \tag{20}$$

First, to obtain the nodal equations for the proposed DNSM, its voltage equations are reformulated as functions of the converter currents. Then, the resultant nonlinear functions of the *qd* ac variables and dc variables are linearized at the time step $(t-\Delta t)$ [41]. The linearized *qd*-dc voltages are written as

$$\begin{bmatrix} v_q^s(t) \\ v_d^s(t) \\ v_{dc}(t) \end{bmatrix} = \begin{bmatrix} R_{qq} & R_{qd} & R_{qdc} \\ R_{dq} & R_{dd} & R_{ddc} \\ R_{dcq} & R_{dcd} & R_{dcdc} \end{bmatrix} \begin{bmatrix} i_q^s(t) \\ i_d^s(t) \\ i_{dc}(t) \end{bmatrix} + \begin{bmatrix} e_{hq}(t) \\ e_{hd}(t) \\ e_{hdc}(t) \end{bmatrix}, \tag{21}$$

where

$$\begin{cases} R_{qq} = \left.\dfrac{\partial v_q^s}{\partial i_q^s}\right|_{t-\Delta t} = R_x\left(w_v(.)\left[w_i(.)\cos(\varphi(.)) + \left(\dfrac{v_{dc}}{R_x} - i_{dc}\right) \times i_d^s \times \dfrac{i_d^s\cos(\varphi(.)) - i_q^s\sin(\varphi(.))}{\left\|\mathbf{i}_{qd}^s\right\|^3}\right]\right)\Bigg|_{t-\Delta t} \\ R_{qd} = \left.\dfrac{\partial v_q^s}{\partial i_d^s}\right|_{t-\Delta t} = R_x\left(w_v(.)\left[w_i(.)\sin(\varphi(.)) + \left(\dfrac{v_{dc}}{R_x} - i_{dc}\right) \times i_q^s \times \dfrac{i_q^s\sin(\varphi(.)) - i_d^s\cos(\varphi(.))}{\left\|\mathbf{i}_{qd}^s\right\|^3}\right]\right)\Bigg|_{t-\Delta t} \\ R_{qdc} = \left.\dfrac{\partial v_q^s}{\partial i_{dc}}\right|_{t-\Delta t} = -R_x\left(w_v(.)\cos\left(\tan^{-1}\left(\dfrac{i_d^s}{i_q^s}\right) - \varphi(.)\right)\right)\Bigg|_{t-\Delta t} \end{cases} \tag{22}$$

$$\begin{cases} R_{dq} = \left.\dfrac{\partial v_d^s}{\partial i_q^s}\right|_{t-\Delta t} = R_x\left(w_v(.)\left[w_i(.)\sin(\varphi(.)) + \left(\dfrac{v_{dc}}{R_x} - i_{dc}\right) \times i_d^s \times \dfrac{i_d^s\sin(\varphi(.)) + i_q^s\cos(\varphi(.))}{\left\|\mathbf{i}_{qd}^s\right\|^3}\right]\right)\Bigg|_{t-\Delta t} \\ R_{dd} = \left.\dfrac{\partial v_d^s}{\partial i_d^s}\right|_{t-\Delta t} = R_x\left(w_v(.)\left[w_i(.)\cos(\varphi(.)) + \left(\dfrac{v_{dc}}{R_x} - i_{dc}\right) \times i_q^s \times \dfrac{i_q^s\cos(\varphi(.)) + i_d^s\sin(\varphi(.))}{\left\|\mathbf{i}_{qd}^s\right\|^3}\right]\right)\Bigg|_{t-\Delta t} \\ R_{ddc} = \left.\dfrac{\partial v_d^s}{\partial i_{dc}}\right|_{t-\Delta t} = -R_x\left(w_v(.)\sin\left(\tan^{-1}\left(\dfrac{i_d^s}{i_q^s}\right) - \varphi(.)\right)\right)\Bigg|_{t-\Delta t} \end{cases} \tag{23}$$

$$\begin{cases} R_{dcq} = \left.\dfrac{\partial v_{dc}}{\partial i_q^s}\right|_{t-\Delta t} = R_x\left(\dfrac{w_v(.)i_q^s}{\left\|\mathbf{i}_{qd}^s\right\|}\right)\Bigg|_{t-\Delta t} \\ R_{dcd} = \left.\dfrac{\partial v_{dc}}{\partial i_d^s}\right|_{t-\Delta t} = R_x\left(\dfrac{w_v(.)i_d^s}{\left\|\mathbf{i}_{qd}^s\right\|}\right)\Bigg|_{t-\Delta t} \\ R_{dcdc} = \left.\dfrac{\partial v_{dc}}{\partial i_{dc}}\right|_{t-\Delta t} = -R_x \end{cases} \tag{24}$$

and

$$\begin{cases} e_{hq}(t) = \left(v_{dc}w_v(.)\cos\left(\tan^{-1}\left(\dfrac{i_d^s}{i_q^s}\right) - \varphi(.)\right)\right)\Bigg|_{t-\Delta t} \\ e_{hd}(t) = \left(v_{dc}w_v(.)\sin\left(\tan^{-1}\left(\dfrac{i_d^s}{i_q^s}\right) - \varphi(.)\right)\right)\Bigg|_{t-\Delta t} \\ e_{hdc}(t) = v_{dc}|_{t-\Delta t} \end{cases} \tag{25}$$

Then, the *qd* variables in (21) are transformed to the *abc* coordinates. After applying Park's inverse transformation to the *qd* variables in (21), and some algebraic manipulations, the equivalent resistance matrix of the converter DNSM in *abc* coordinates yields

$$\mathbf{R}_{\text{CON}} = \begin{bmatrix} R_{aa} & R_{ab} & R_{ac} & R_{adc} \\ R_{ba} & R_{bb} & R_{bc} & R_{bdc} \\ R_{ca} & R_{cb} & R_{cc} & R_{cdc} \\ R_{dca} & R_{dcb} & R_{dcc} & R_{dcdc} \end{bmatrix} = \begin{bmatrix} [\mathbf{K}(\theta_s)]^{-1}\begin{bmatrix} R_{qq} & R_{qd} \\ R_{dq} & R_{dd} \end{bmatrix}[\mathbf{K}(\theta_s)] & [\mathbf{K}(\theta_s)]^{-1}\begin{bmatrix} R_{qdc} \\ R_{ddc} \end{bmatrix} \\ -\left(\begin{bmatrix} R_{dcq} & R_{dcd} \end{bmatrix}[\mathbf{K}(\theta_s)]\right) & R_{dcdc} \end{bmatrix}. \tag{26}$$

Here, the positive dc current is considered outward of the converter. Therefore, a negative sign is used with the dc-*abc* equivalent resistances to account for this convention.

Also, the vector of voltage history terms $\mathbf{e}_{h\text{CON}}$ in *abc* coordinates is obtained as

$$\mathbf{e}_{h\text{CON}} = \begin{bmatrix} e_{ha}(t) \\ e_{hb}(t) \\ e_{hc}(t) \\ e_{hdc}(t) \end{bmatrix} = \begin{bmatrix} [\mathbf{K}(\theta_s)]^{-1}\begin{bmatrix} e_{hq}(t) \\ e_{hd}(t) \end{bmatrix} \\ e_{hdc}(t) \end{bmatrix}. \tag{27}$$

To organize the equations in the form of (17), the converter conductance matrix $\mathbf{G}_{\text{CON}}$ and history currents $\mathbf{I}_{h\text{CON}}$ are calculated as [41]

$$\mathbf{G}_{\text{CON}} = [\mathbf{R}_{\text{CON}}]^{-1}, \tag{28}$$

and

$$\mathbf{I}_{h\text{CON}} = -[\mathbf{R}_{\text{CON}}]^{-1}\mathbf{e}_{h\text{CON}}. \tag{29}$$

The equivalent conductance matrix $\mathbf{G}_{\text{CON}}$ calculated using (22)(23), (24), (26), (28) and vector of current history terms $\mathbf{I}_{h\text{CON}}$ calculated using (21)–(27), (29) are then directly incorporated into the overall network nodal equations (17) when the EMT program permits. Alternatively, the proposed DI-DNSM can be interfaced using circuit components according to Fig. 8 based on its Norton equivalent circuit.

As demonstrated in Fig. 8, in contrast to the indirect interfacing method shown in Fig. 7, the external snubber and compensation current are not required for the DI-DNSM as the model is already integrated into the nodal formulation. Furthermore, no input variables from the previous time step are required, and the simultaneous solution of the converter's nodal equations with the overall network variables is achieved.

The flowchart in Fig. 9 summarizes the procedure for implementing the proposed DI-DNSM in an EMTP-type solution. As depicted in Fig. 9, the nodal equations of the overall network are solved to determine the node voltages. Subsequently, the converter currents are calculated based on the obtained voltages. With the voltages and currents of the ac and dc subsystems available, the instantaneous dynamic impedance can be determined at any moment during the

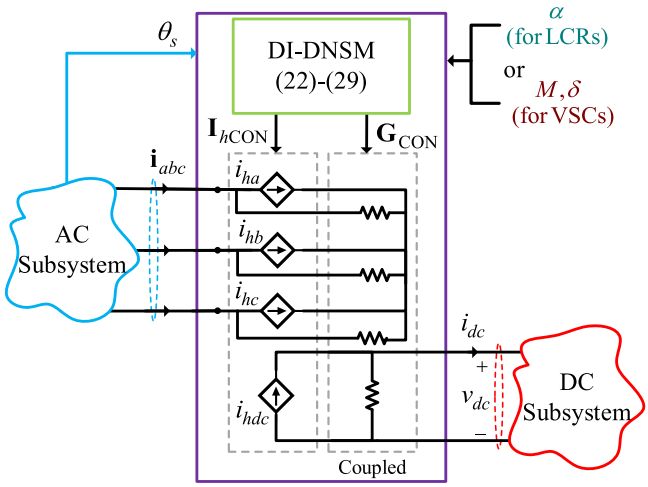

FIGURE 8. Direct interfacing of the proposed DNSM with the external network using Norton equivalent circuit.

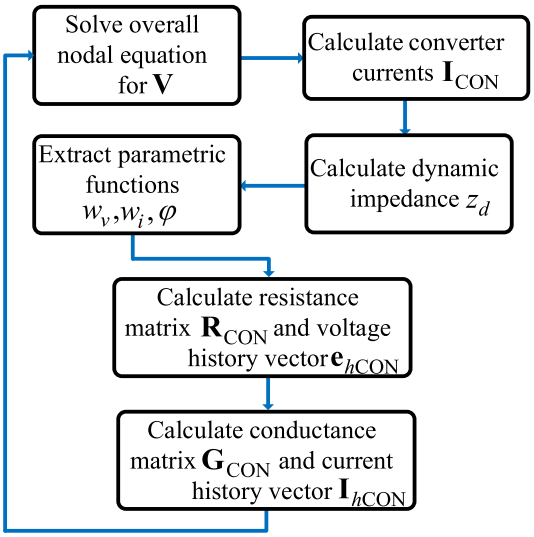

FIGURE 9. Flowchart of procedure for implementing the proposed DI-DNSM in EMTP-type solution.

simulation. Using this impedance, in conjunction with other parameters (such as the firing angle of thyristor-based converters), values of parametric functions are computed from lookup tables at each simulation time step. The converter resistance matrix and voltage history terms are computed as the Thevenin equivalent of the converter equations. Then, the Norton equivalent of the model is calculated to obtain the conductance matrix and current histories/injections, which are then incorporated into the overall nodal equations. This procedure is repeated at every simulation time step.

IV. COMPUTER STUDIES

To investigate the performance of the proposed modeling approach against the conventional detailed switching models of LCRs and VSCs, the ac–dc system in Fig. 1 is considered with diode- and thyristor-based LCRs, as well as VSC. The system parameters are summarized in the Appendix.

The systems with the conventional DSM of the converters have been implemented in PSCAD (offline) and RSCAD (real-time) using their standard library components. Also, the proposed DNSM is implemented in PSCAD with the indirect and direct interfacing methods, denoted as IDI-DNSM and DI-DNSM, respectively. The IDI-DNSM of the LCRs and VSCs presented in Section III-A is also implemented using basic library components of PSCAD based on Figs. 6 and 7. The DI-DNSM presented in Section III-B is implemented as a PSCAD user-defined block by defining a conductance G matrix and a vector of history currents based on (26)–(29) and Fig. 8.

All the simulations with LCRs in PSCAD are run with disabled interpolation for the switching events for consistency with real-time simulations in RSCAD. Also, to enhance the numerical stability of the DSM in simulations without switching interpolations, artificial snubber circuits are used for the switches in the DSM for fair comparisons [47].

A. STUDIES WITH DIODE- LCR

Here, it is assumed that the LCR in Fig. 1 consists of six diodes. The system is initially in steady-state with the LCR operating in CCM-1 mode supplying a load with $R_l = 5\,\Omega$ and $L_l = 2\,\text{mH}$. At $t = 2\,s$, the load is stepped down to $R_l = 0.5\,\Omega$, which changes the operating mode of the LCR to CCM-2. The transient response of the ac and dc variables obtained by the four subject models (i.e., DSM in PSCAD, DSM in RSCAD, and the proposed IDI- and DI-DSM in PSCAD) are shown in Fig. 10.

The results in Fig. 10 are obtained when the DSM in PSCAD and RSCAD are both run with a time-step of $\Delta t = 10\,\mu\text{s}$, which was the maximum possible time-step to achieve accurate results without interpolations. The two proposed IDI-DNSM and DI-DNSM are able to use much larger time steps and are run with $\Delta t = 70\,\mu\text{s}$ and $\Delta t = 200\,\mu\text{s}$, respectively.

As can be observed in Fig. 10, the simulation results with the DSM run in offline mode (using PSCAD) and in real-time mode (using RSCAD) match almost precisely. It is also verified that the proposed IDI-DNSM and DI-DNSM are able to provide an accurate reconstruction of the entire ac and dc waveforms, consistent with the switching models, both in steady-state and in transients using much larger time steps (i.e., 70 μs and 200 μs, respectively).

Fig. 11 depicts the waveforms of the diode LCR obtained by the conventional DSM and the proposed IDI-DNSM while both simulations are conducted in real-time using RSCAD with 70 μs time-step. As can be observed, the conventional DSM cannot accurately reproduce the ac and dc waveforms at such large time steps due to the errors in handling switching events; however, the proposed DNSM still achieves accurate results, similar to the waveforms in Fig. 10.

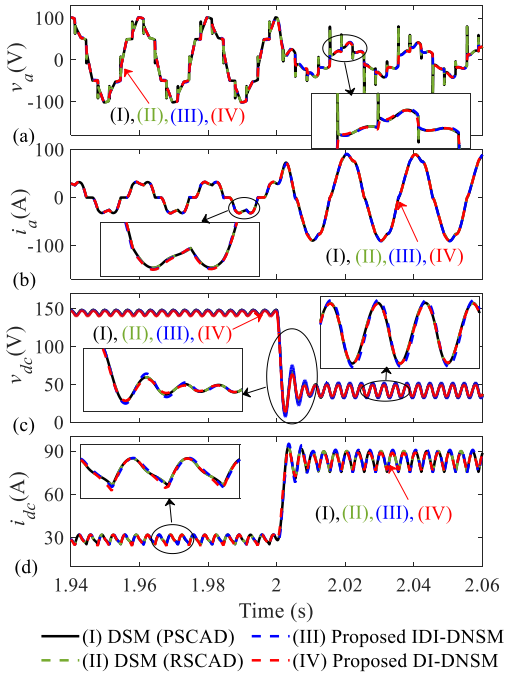

FIGURE 10. Transient response of diode LCR variables as obtained by the subject models for: (a) phase *a* voltage v_a, (b) phase *a* current i_a, (c) dc voltage v_{dc}, and (d) dc current i_{dc}. The DSMs in PSCAD and RSCAD are run with $\Delta t = 10\,\mu$s, IDI-DNSM with $\Delta t = 70\,\mu$s, and DI-DNSM with $\Delta t = 200\,\mu$s.

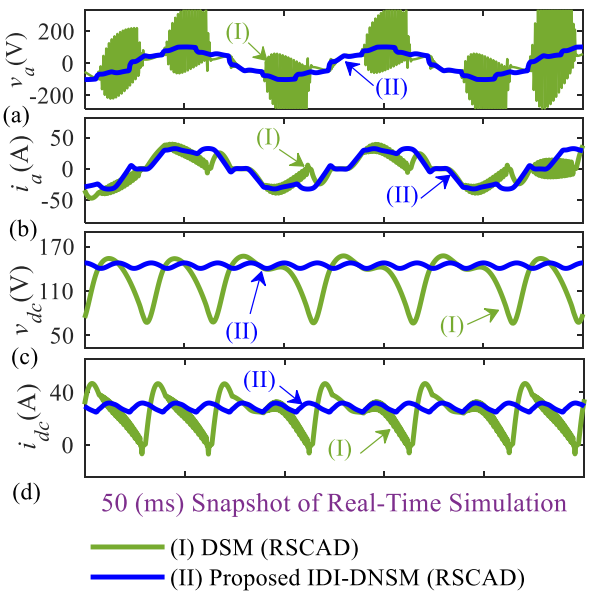

FIGURE 11. Steady-state waveforms of ac- and dc-side variables of diode LCR in CCM-1 condition as obtained by the conventional DSM and proposed IDI-DNSM run on RSCAD with $\Delta t = 70\,\mu$s: (a) phase *a* voltage v_a, (b) phase *a* current i_a, (c) dc voltage v_{dc}, and (d) dc current i_{dc}.

B. STUDIES WITH THYRISTOR-LCR

Here, it is assumed that the LCR in the system of Fig. 1 is composed of controlled thyristor switches. Initially, the system is in steady-state with the LCR operating in CCM-1 mode where the firing angle of thyristors is set to $\alpha = 35^\circ$, and the

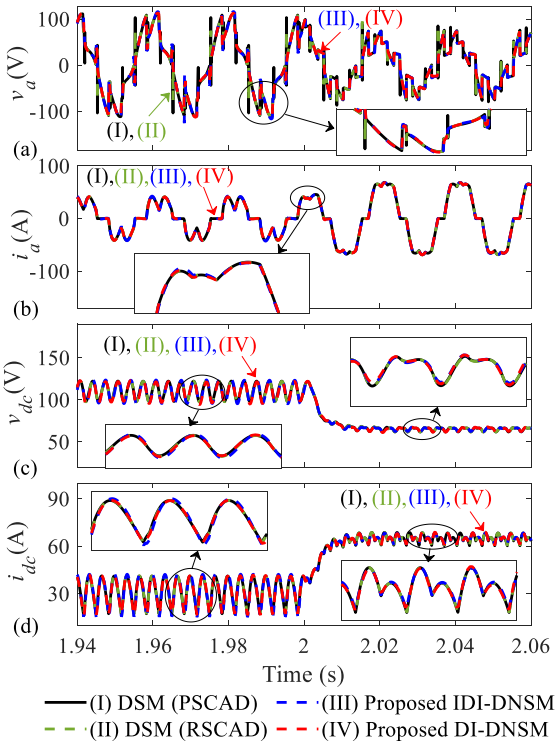

FIGURE 12. Transient response of thyristor LCR variables as obtained by the subject models for: (a) phase *a* voltage v_a, (b) phase *a* current i_a, (c) dc voltage v_{dc}, and (d) dc current i_{dc}. The DSMs in PSCAD and RSCAD are run with $\Delta t = 10\,\mu$s, IDI-DNSM with $\Delta t = 50\,\mu$s, and DI-DNSM with $\Delta t = 150\,\mu$s.

LCR feeds a series *RL* load with $R_l = 3.5\,\Omega$ and $L_l = 10$ mH. Then, at $t = 2\,s$, the dc load resistance is stepped to $R_l = 1\,\Omega$ and the firing angle steps to $\alpha = 15^\circ$.

The transient response is shown in Fig. 12 as obtained by the DSM in RSCAD and PSCAD (with $\Delta t = 10\,\mu$s), the proposed IDI-DNSM (with $\Delta t = 50\,\mu$s), and the proposed DI-DNSM (with $\Delta t = 150\,\mu$s).

In line with the observations in Fig. 10 for the diode-LCR, it is observed in Fig. 12 that the results with the DSM run in offline mode (using PSCAD) and in real-time mode (using RSCAD) are consistent. It is also seen that the proposed IDI-DNSM and DI-DNSM are able to capture the entire ac and dc waveforms (including their ripples, harmonics, sharp edges, etc.) consistently with the switching models, both in steady-state and in transients. It is emphasized that the IDI-DNSM and DI-DNSM achieve this with such large time-step sizes (i.e., 50 μs and 150 μs, respectively), which is a significant numerical advantage over the DSM, which can run only with small time-steps (10 μs).

C. STUDIES WITH VSC

Here, the VSC in the system of Fig. 1 is considered to have a conventional two-level topology. The switching frequency f_c is assumed to be 900 Hz using the sinusoidal pulse-width modulation (SPWM). The simulation starts from zero initial

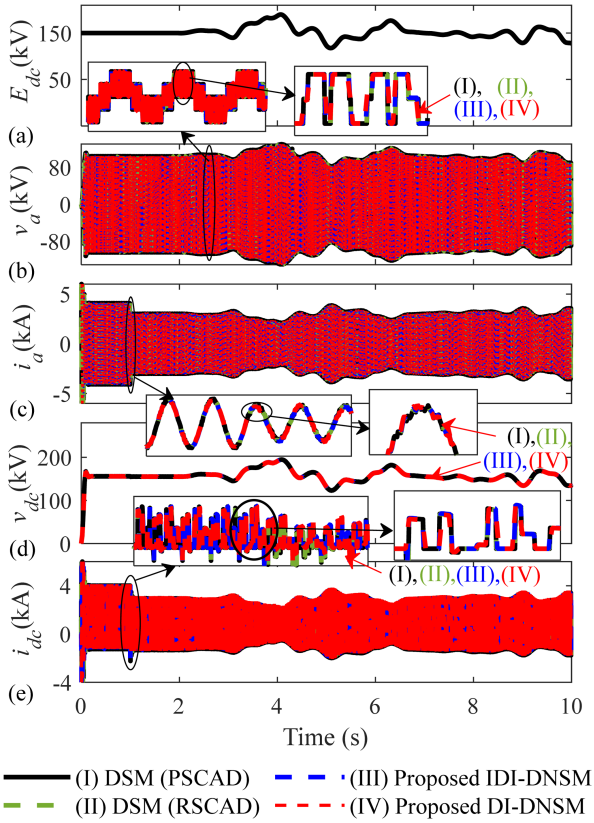

FIGURE 13. Transient response of VSC variables as obtained by the subject models for: (a) dc subsystem voltage source E_{dc}, (b) phase a voltage v_a, (c) phase a current i_a, (d) dc voltage v_{dc}, and (e) dc current i_{dc}. The DSMs in PSCAD and RSCAD are run with $\Delta t = 10\,\mu$s, IDI-DNSM with $\Delta t = 25\,\mu$s, and DI-DNSM with $\Delta t = 50\,\mu$s.

condition while the modulation index and angle are set to $M = 0.6$ and $\delta = -15^\circ$, transferring 80 MW in steady-state from the ac subsystem to the dc subsystem. Without loss of generality, the dc subsystem here is composed of a series RL branch with $R_l = 5.99\,\Omega$ and $L_l = 84\,$mH, and dc voltage source $E_{dc} = 150$ kV, representing the inverter side of an HVDC system. Then, at $t = 1\,s$, the modulation index and angle are stepped to $M = 0.8$ and $\delta = -10^\circ$, decreasing the transferred power to 70MW. Then, at $t = 2\,s$, the dc subsystem voltage source E_{dc} starts to fluctuate based on the profile in Fig. 13(a). The transient response of the system variables is depicted in Fig. 13(b)–(e), where the results of the DSM in RSCAD and PSCAD are obtained with $\Delta t = 10\,\mu$s, and proposed IDI-DNSM and DI-DNSM with $\Delta t = 25\mu$s and $\Delta t = 50\,\mu$s, respectively.

It can be observed in Fig. 13 that the proposed IDI-DNSM and DI-DNSM accurately replicate the entire ac and dc waveforms, aligning with the DSMs. This accuracy is maintained in steady-state and transients, with larger time-step sizes of 25 μs and 50 μs for IDI-DNSM and DI-DNSM, respectively, achieving numerical advantages.

For the DSM of the VSC system in this paper, an accurate solution cannot be obtained without interpolation, even at very small time steps $\Delta t < 0.01\,\mu$s, due to high-frequency switching. Therefore, the DSM of VSC in PSCAD is presented here with interpolation enabled to verify the solution provided by the proposed models. Also, the RSCAD DSM is implemented using their substep 2-level VSC [48].

TABLE 1. Maximum Possible Simulation Time-Step With the Subject Models of LCR and VSC Systems

Converter Model	Max Time-Step Size (μs)		
	Diode-based LCR	Thyristor-based LCR	VSC
Conventional DSM*	10	10	$\Delta t < 0.01$ (Individual switch-based model) 10 (substep VSC in RSCAD)
Proposed IDI-DNSM	70	50	25
Proposed DI-DNSM	200	150	50

*Artificial snubbers are enabled for DSMs for numerical damping.

TABLE 2. Computational Performance of Conventional Switching and Proposed Non-Switching Detailed Models of Diode and Thyristor LCRs and VSC Systems for the 30-Second Transient Study in PSCAD

Converter	Δt (μs)	CPU Time (s)		
		DSM	Proposed IDI-DNSM	Proposed DI-DNSM
Diode-based LCR	10	16.4	20.7	28.6
	70	NA	3.02	4.2
	200	NA	NA	1.9
Thyristor-based LCR	10	19.6	20.7	28.6
	50	NA	4.2	5.8
	150	NA	NA	2.1
VSC	10	43.1	37.2	42.3
	25	NA	15.9	18.6
	50	NA	NA	10.1

The maximum possible time-step sizes to obtain numerically valid results with the subject models are summarized in Table 1. As seen, the conventional DSM, IDI-DNSM, and DI-DNSM are valid up to 10 μs, 70 μs, and 200 μs for the diode-based LCR system, respectively; 10 μs, 50 μs, and 150 μs for the thyristor-based LCR system, respectively; and 10 μs, 25 μs, and 50 μs for the VSC system, respectively.

D. COMPUTATIONAL PERFORMANCE COMPARISON

Here, the computational performance of the IDI-DNSM and DI-DNSM is benchmarked against the conventional DSM of LCR and VSC systems. The offline CPU times taken with the three subject models to run identical 30-second transient studies discussed in Sections IV-A, IV-B, and IV-C with different time-step sizes are summarized in Table 2 for the diode LCR, thyristor LCR, and VSC systems, respectively. These CPU times are available in the PSCAD build message pane after each simulation.

As observed in Table 2, with $\Delta t = 10\,\mu$s, the proposed IDI-DNSM of diode and thyristor LCRs is computationally as expensive as the conventional DSM (taken 20.7s and 16.4s

CPU time for diode LCR and 20.7s and 19.6s for thyristor LCR, respectively). In contrast, the proposed DI-DNSM requires slightly more computations (i.e., 28.6s CPU time for diode LCR and 28.6s for thyristor LCR). However, the proposed IDI-DNSM and DI-DNSM can run with larger time steps. For the diode LCR system with $\Delta t = 70\,\mu$s, they can run in 3.02s and 4.2s, respectively. Also, for the thyristor-based system at $\Delta t = 50\,\mu$s, 4.2s and 5.8s CPU times are required for IDI-DNSM and DI-DNSM, respectively. The DI-DNSM can be simulated with even larger time-steps of up to $\Delta t = 200\,\mu$s for diode LCR and $\Delta t = 150\,\mu$s for thyristor LCR for which only 1.9s and 2.1s is taken by the CPU, respectively.

For the VSC system, it is seen in Table 2 that the conventional DSM requires 43.1s CPU time with $\Delta t = 10\,\mu$s. It is noted that this time step was possible only by enabling the switching interpolation, without which the time step would have been limited to less than 0.01 μs. The proposed IDI-DNSM and DI-DNSM also have comparable performance and required 37.2s and 42.3s, respectively. The IDI-DNSM and DI-DNSM can also run faster (i.e., 15.9s and 18.6s) by increasing the time-step to $\Delta t = 25\mu$s. The proposed DI-DNSM is even able to run with $\Delta t = 50\,\mu$s in only 10.1s.

V. DISCUSSIONS

It is worth mentioning that the methodology presented in this paper can be applied to other types of converters. For instance, the parametric functions for the DNSM of line-commutated inverters or voltage-source inverters with different modulation strategies can be defined in a similar procedure to that outlined in this paper with respect to the instantaneous values of the converter variables. Once these instantaneous parametric functions are established for the considered converter, the DI-DNSM of such converters can also be formulated as in (28) and (29). This enables their incorporation into the external network equations in EMTP-type programs in accordance with the process outlined in Fig. 9.

It is also worth mentioning that the proposed model can replicate any feature of detailed switching models if the reference model used to generate the lookup tables includes them. This encompasses features like dead bands, transients occurring within the time range of the switching period, etc. However, while DNSM excels at predicting the accurate values of converter variables at any moment in fixed-time step simulations, the precise moment of switching is unknown to the model in situations where switching events occur within a time-step interval. Some predictive algorithms, such as the improved firing of UCM in RSCAD, have been developed to accurately predict the switching moment with high precision [49]. Taking inspiration from the UCM algorithm, a modified predictive DNSM based on predefined parametric functions could be developed to enhance the accuracy of the model.

Additionally, the development of an optimal algorithm for lookup table construction can be an intriguing study aimed at streamlining the initial stage of the proposed methodology to avoid any unnecessary primary computation and memory occupation.

VI. CONCLUSION

This paper has proposed a new technique for modeling ac–dc switching converters in EMT simulators. The proposed technique can provide detailed waveforms consistent with the conventional switching models of converters and be used in simulations with large time steps. This was achieved by formulating parametric functions that instantaneously relate the converter's ac and dc variables. Two interfacing methods were presented for the proposed models. With the indirect interfacing method, the proposed model was able to provide accurate results with time steps up to $\sim$70 μs for diode and thyristor-based LCR systems, and up to $\sim$30 μs for VSC-based systems. Meanwhile, the proposed model with direct interfacing could accurately run with time steps up to $\sim$200 μs for LCRs, and up to $\sim$50 μs for VSCs. The proposed methodology has been demonstrated to surpass conventional detailed switching models in terms of computational speed while providing sufficiently accurate solutions. This is especially valuable in real-time applications where achieving efficient performance with a non-iterative solution is highly desirable.

APPENDIX

LCR system parameters:

$$E_{rms} = 90\,\text{V},\quad f_e = 50\,\text{Hz},\quad r_s = 1\,\Omega,\quad L_s = 1\,\text{mH},$$
$$C_f = 500\ \mu\text{F},\ R_x = 100\,\Omega\,,$$
$$R_{on\_switch} = 0.091\,\Omega,\quad V_{on\_switch} = 0.637\,\text{V}.$$

VSC system parameters:

$$E_{rms} = 70.7\,\text{kV},\quad f_e = 60\,\text{Hz},\ f_c = 900\ \text{Hz},\quad r_s = 1.5\,\Omega,$$
$$L_s = 37.14\,m\text{H},\ C_f = 3000\ \mu\text{F}, R_x = 150\ \Omega\,.$$

REFERENCES

[1] N. Mohan, T. M. Undeland, and W. P. Robbins, *Power Electronics*, 3rd ed. Hoboken, NJ, USA: Wiley, 2003.

[2] W. Wang, A. Beddard, M. Barnes, and O. Marjanovic, "Analysis of active power control for VSC–HVDC," *IEEE Trans. Power Del.*, vol. 29, no. 4, pp. 1978–1988, Aug. 2014.

[3] T. Abedin et al., "Dynamic modeling of HVDC for power system stability assessment: A review, issues, and recommendations," *Energies*, vol. 14, no. 16, pp. 4829–4854, Aug. 2021.

[4] H. Rao et al., "Design aspects of hybrid HVDC system," *CSEE J. Power Energy Syst.*, vol. 7, no. 3, pp. 644–653, May 2021.

[5] N. Flourentzou, V. G. Agelidis, and G. D. Demetriades, "VSC-based HVDC power transmission systems: An overview," *IEEE Trans. Power Electron.*, vol. 24, no. 3, pp. 592–602, Mar. 2009.

[6] B. He and M. Yang, "Robust LPV control of diesel auxiliary power unit for series hybrid electric vehicles," *IEEE Trans. Power Electron.*, vol. 21, no. 3, pp. 791–798, May 2006.

[7] A. Jimenez and N. García, "Power flow modeling and analysis of voltage source converter-based plug-in electric vehicles," in *Proc. IEEE Power Energy Soc. Gen. Meeting*, 2011, pp. 1–6.

[8] İ. Yılmaz, M. Ermiş, and I. Çadırcı, "Medium frequency induction melting furnace as a load on the power system," in *Proc. IEEE Ind. Appl. Soc. Annu. Meeting*, 2011, pp. 1–12.

[9] S. Zhu, C. Liu, K. Wang, Z. Zhou, and J. Yu, "Structure and operating performance of a double electrical excitation synchronous generator with embedded brushless synchronous exciter utilizing DC-field excitation," *IEEE Trans. Energy Convers.*, vol. 37, no. 1, pp. 50–64, Mar. 2022.
[10] J. Sottile, F. C. Trutt, and A. W. Leedy, "Condition monitoring of brushless three-phase synchronous generators with stator winding or rotor circuit deterioration," *IEEE Trans. Ind. Appl.*, vol. 42, no. 5, pp. 1209–1215, Sep./Oct. 2006.
[11] Y. Zhang and A. M. Cramer, "Numerical average-value modeling of rotating rectifiers in brushless excitation systems," *IEEE Trans. Energy Convers.*, vol. 32, no. 4, pp. 1592–1601, Dec. 2017.
[12] *Guidance Notes on Control of Harmonics in Electrical Power System*, Houston, TX, USA: Amer. Bureau Shipping, May 2006.
[13] M. H. Bierhoff and F. W. Fuchs, "DC-link harmonics of three-phase voltage-source converters influenced by the pulsewidth-modulation strategy—An analysis," *IEEE Trans. Ind. Electron.*, vol. 55, no. 5, pp. 2085–2092, May 2008.
[14] M. E. Villablanca, "Harmonic-free line-commutated ac/dc rectifiers," *Electric Power Syst. Res.*, vol. 79, no. 11, pp. 1531–1537, Nov. 2009.
[15] A. M. Gole, S. Filizadeh, R. W. Menzies, and P. L. Wilson, "Optimization enabled electromagnetic transient simulation," *IEEE Trans. Power Del.*, vol. 20, no. 1, pp. 512–518, Jan. 2005.
[16] A. M. Gole, I. T. Fernando, G. D. Irwin, and O. B. Nayak, "Modeling of power electronic apparatus: Additional interpolation issues," in *Proc. Int. Conf. Power Syst. Transients*, 1997, pp. 23–28.
[17] G. Irwin, D. Woodford, and A. Gole, "Precision simulation of PWM controllers," in *Proc. Int. Conf. Power Syst. Transients*, 2001, pp. 1–5.
[18] T. Maguire and J. Giesbrecht, "Small time-step (<2 μ Sec) VSC model for the real time digital simulator," in *Proc. Int. Conf. Power Syst. Transients*, 2005, pp. 1–6.
[19] T. Maguire, S. Elimban, E. Tara, and Y. Zhang, "Predicting switch ON/OFF statuses in real time electromagnetic transients simulations with voltage source converters," in *Proc. IEEE 2nd Conf. Energy Internet Energy Syst. Integration*, 2018, pp. 1–7.
[20] K. L. Lian and P. W. Lehn, "Real-time simulation of voltage source converters based on time average method," *IEEE Trans. Power Syst.*, vol. 20, no. 1, pp. 110–118, Feb. 2005.
[21] P. M. Menghal and A. J. Laxmi, "Real time simulation: Recent progress & challenges," in *Proc. IEEE Int. Conf. Power, Signals, Controls Comput.*, 2012, pp. 1–6.
[22] M. D. Omar Faruque et al., "Real-time simulation technologies for power systems design, testing, and analysis," *IEEE Power Energy Technol. Syst. J.*, vol. 2, no. 2, pp. 63–73, Jun. 2015.
[23] Y. Huang, L. Dong, S. Ebrahimi, N. Amiri, and J. Jatskevich, "Dynamic phasor modeling of line-commutated rectifiers with harmonics using analytical and parametric approaches," *IEEE Trans. Energy Convers.*, vol. 32, no. 2, pp. 534–547, Jun. 2017.
[24] M. Daryabak, S. Filizadeh, and A. Bagheri Vandaei, "Dynamic phasor modeling of LCC-HVDC systems: Unbalanced operation and commutation failure," *Can. J. Elect. Comput. Eng.*, vol. 42, no. 2, pp. 121–131, Spring 2019.
[25] D. Shu, Y. Wei, V. Dinavahi, K. Wang, Z. Yan, and X. Li, "Cosimulation of shifted-frequency/dynamic phasor and electromagnetic transient models of hybrid LCC-MMC DC grids on integrated CPU–GPUs," *IEEE Trans. Ind. Electron.*, vol. 67, no. 8, pp. 6517–6530, Aug. 2020.
[26] P. De Rua, Ö. C. Sakinci, and J. Beerten, "Comparative study of dynamic phasor and harmonic state-space modeling for small-signal stability analysis," *Electric Power Syst. Res.*, vol. 189, 2020, Art. no. 106626.
[27] S. D. Sudhoff, "Analysis and average-value modeling of line-commutated converter—Synchronous machine systems," *IEEE Trans. Energy Convers.*, vol. 8, no. 1, pp. 92–99, Mar. 1993.
[28] S. D. Sudhoff, "Waveform reconstruction from the average-value model of line-commutated converter-synchronous machine system," *IEEE Trans.Energy Convers.*, vol. 8, no. 3, pp. 404–410, Sep. 1993.
[29] J. T. Alt, S. D. Sudhoff, and B. E. Ladd, "Analysis and average-value modeling of an inductorless synchronous machine load commutated converter system," *IEEE Trans. Energy Convers.*, vol. 14, no. 1, pp. 37–43, Mar. 1999.
[30] S. D. Sudhoff, K. A. Corzine, H. J. Hegner, and D. E. Delisle, "Transient and dynamic average-value modeling of synchronous machine fed load-commutated converters," *IEEE Trans. Energy Convers.*, vol. 11, no. 3, pp. 508–514, Sep. 1996.
[31] J. Jatskevich, S. D. Pekarek, and A. Davoudi, "Fast procedure for constructing an accurate dynamic average-value model of synchronous machine-rectifier system," *IEEE Trans. Energy Convers.*, vol. 21, no. 2, pp. 435–441, Jun. 2006.
[32] M. Shahnazari and A. Vahedi, "Improved dynamic average value modeling of brushless excitation system in all rectification modes," *IET Elect. Power Appl.*, vol. 4, pp. 657–669, Sep. 2010.
[33] S. Chiniforoosh et al., "Definitions and applications of dynamic average models for analysis of power systems," *IEEE Trans. Power Del.*, vol. 25, no. 4, pp. 2655–2669, Oct. 2010.
[34] J. Jatskevich, S. D. Pekarek, and A. Davoudi, "Parametric average-value model of synchronous machine-rectifier systems," *IEEE Trans. Energy Convers.*, vol. 21, no. 1, pp. 9–18, Mar. 2006.
[35] P. Norman, J. T. Alt, and G. Burt, "Parametric average-value converter modeling for aerospace applications," *SAE Int. J. Aerosp.*, vol. 5, pp. 318–324, Oct. 2012.
[36] Y. Zhang and A. M. Cramer, "Formulation of rectifier numerical average-value model for direct interface with inductive circuitry," *IEEE Trans. Energy Convers.*, vol. 34, no. 2, pp. 741–749, Jun. 2019.
[37] S. Ebrahimi, N. Amiri, H. Atighechi, Y. Huang, L. Wang, and J. Jatskevich, "Generalized parametric average-value model of line-commutated rectifiers considering AC harmonics with variable frequency operation," *IEEE Trans. Energy Convers.*, vol. 33, no. 1, pp. 341–353, Mar. 2018.
[38] S. Ebrahimi, N. Amiri, and J. Jatskevich, "Hybrid parametric average-value/detailed modeling of line-commutated rectifiers," *IEEE Trans. Energy Convers.*, vol. 35, no. 3, pp. 1494–1504, Sep. 2020.
[39] ARTEMiS CPU-based electrical Toolbox. [Online]. Available: https://www.opal-rt.com/solver/
[40] EMTDC User's Guide v4.6, chapter 4, Interpolation and switching, 2018. [Online]. Available: https://www.pscad.com/knowledge-base/article/163
[41] S. Ebrahimi, H. Atighechi, S. Chiniforoosh, and J. Jatskevich, "Direct interfacing of parametric average-value models of AC–DC converters for nodal analysis-based solution," *IEEE Trans. Energy Convers.*, vol. 37, no. 4, pp. 2408–2418, Dec. 2022.
[42] S. Ebrahimi and J. Jatskevich, "Average-value model for voltage-source converters with direct interfacing in EMTP-type solution," *IEEE Trans. Energy Convers.*, vol. 38, no. 3, pp. 2231–2234, Sep. 2023.
[43] P. C. Krause, O. Wasynczuk, S. D. Sudhoff, and S. Pekarek, *Analysis of Electric Machinery and Drive Systems*, 3rd ed. Piscataway, NJ, USA: Wiley, 2013.
[44] D. G. Holmes and T. A. Lipo, *Pulse Width Modulation For Power Converters: Principles and Practice*, 1st ed. New York, NY, USA: Wiley, 2003.
[45] N. G. Hingorani and L. Gyugyi, *Understanding FACTS: Concepts and Technology of Flexible AC Transmission Systems*, 1st ed. New York, NY, USA: Wiley, 1999.
[46] S. Ebrahimi, N. Amiri, and J. Jatskevich, "Interfacing of parametric average-value models of LCR systems in fixed-time-step real-time EMT simulations," *IEEE Trans. Energy Convers.*, vol. 35, no. 4, pp. 1985–1988, Dec. 2020.
[47] S. Ebrahimi, N. Amiri, J. Jatskevich, and L. Wang, "Simulation of line-commutated rectifier systems using fixed time-dtep without zero-crossing events," in *Proc. IEEE Int. Conf. Smart Energy Grid Eng.*, 2018, pp. 195–199.
[48] "Substep: High-fidelity simulation and testing of power electronics," [Online]. Available: https://knowledge.rtds.com/hc/en-us/article_attachments/360048465654
[49] "The Universal Converter Model for enhanced real-time power electronics simulation," [Online]. Available: https://www.rtds.com/ucm/

PARASTOO SADAT HOSSEINIAN (Student Member, IEEE) received the B.Sc. and M.Sc. degrees in electrical engineering from the Amirkabir University of Technology, Tehran, Iran, in 2017 and 2019, respectively, and the M.A.Sc. degree in electrical and computer engineering from The University of British Columbia, Vancouver, BC, Canada, in 2023. Her research interests include modeling and analysis of power electronic converters, power system operation and planning, and power system resiliency.

SEYYEDMILAD EBRAHIMI (Member, IEEE) received the B.Sc. and M.Sc. degrees in electrical engineering from the Sharif University of Technology, Tehran, Iran, in 2010 and 2012, respectively, and the Ph.D. degree in electrical and computer engineering from The University of British Columbia (UBC), Vancouver, BC, Canada, in 2019. He is currently a Postdoctoral Teaching and Research Fellow with the Department of Electrical and Computer Engineering, UBC. His research interests include modeling and analysis of power electronic converters and electrical machines, application of power electronics to power systems, modeling and control of power systems, and simulation of electromagnetic transients.

JURI JATSKEVICH (Fellow, IEEE) received the M.S.E.E. and the Ph.D. degrees in electrical engineering from Purdue University, West Lafayette IN, USA, in 1997 and 1999, respectively. Since 2002, he has been with The University of British Columbia, Vancouver, BC, Canada, where he is currently a Professor with the Department of Electrical and Computer Engineering. His research interests include power electronic systems, electrical machines and drives, modeling and simulation of electromagnetic transients. Dr. Jatskevich was an Associate Editor for IEEE TRANSACTIONS ON POWER ELECTRONICS during 2008–2013, the Editor-in-Chief of the IEEE TRANSACTIONS ON ENERGY CONVERSION during 2013–2019, and Editor-in-Chief At-Large of the IEEE PES journals in 2019 and 2020. He is also chairing the IEEE Task Force on Dynamic Average Modeling, under Working Group on Modeling and Analysis of System Transients Using Digital Programs. He was the recipient of the 2022 IEEE PES Cyril Veinott Electromechanical Energy Conversion Award.